

Distributed Frequency Control of Heterogeneous Energy Storage Systems Considering Short-Term Ability and Long-Term Flexibility

Ruiwen Liu^{ID}, Graduate Student Member, IEEE, Hongxun Hui^{ID}, Member, IEEE, Xia Chen^{ID}, Member, IEEE, and Yonghua Song^{ID}, Fellow, IEEE

Abstract—Renewable energy sources introduce more fluctuations into the power system and bring challenges to maintain the system stability. Conventional generation units are gradually replaced and may soon become inadequate to meet the frequency regulation (FR) requirements. Consequently, demand-side resources for FR have received increasing attention. Among demand-side sources, inverter air conditioners (IACs) have huge regulation capacity and account for nearly 40% of the total power consumption in summer, while energy storage systems (ESSs) excel in rapid response and powerful ramp rate. However, the inadequate ramp speed of IACs and the insufficient regulation capacity of ESSs render them incapable of providing FR independently. To tackle this problem, this paper proposes a distributed coordinated control algorithm that allows the effective utilization of ESSs and IACs to provide FR considering the respective advantages. Firstly, an equivalent thermal energy storage model of IAC in alignment with ESS is introduced considering heterogeneous parameters. Subsequently, a coordinated control framework is proposed for heterogeneous ESSs (hetero-ESSs), which are composed of ESSs and IACs. Based on the framework, a distributed consensus algorithm is devised for hetero-ESSs, and its stability is demonstrated through the application of the Lyapunov theorem. Finally, numerical studies verify that the proposed framework can promote ESSs' short-term ability and IACs' long-term flexibility.

Index Terms—Distributed control, frequency regulation, energy storage system, inverter air conditioner, Lyapunov stability.

Manuscript received 18 October 2023; revised 2 April 2024 and 5 June 2024; accepted 20 July 2024. Date of publication 29 August 2024; date of current version 23 October 2024. This work was supported in part by the National Natural Science Foundation of China under Grant 52407075 and Grant U22A6007; in part by the Guangdong Basic and Applied Basic Research Foundation, China, under Grant 2024A1515010141; in part by the Science and Technology Development Fund, Macau, SAR, under Grant 001/2024/SKL and Grant 0117/2022/A3, and in part by the Chair Professor Research Grant of University of Macau under Grant CPG2024-00015-IOTSC. Paper no. TSG-01704-2023. (Corresponding author: Hongxun Hui.)

Ruiwen Liu, Hongxun Hui, and Yonghua Song are with the State Key Laboratory of Internet of Things for Smart City and the Department of Electrical and Computer Engineering, University of Macau, Macau, China, and also with the Zhuhai UM Science and Technology Research Institute, Zhuhai 519031, China (e-mail: hongxunhui@um.edu.mo).

Xia Chen is with the State Key Laboratory of Advanced Electromagnetic Engineering and Technology and the School of Electrical and Electronic Engineering, Huazhong University of Science and Technology, Wuhan 430074, China.

Color versions of one or more figures in this article are available at <https://doi.org/10.1109/TSG.2024.3451614>.

Digital Object Identifier 10.1109/TSG.2024.3451614

NOMENCLATURE

Abbreviation

DCA	Distributed consensus algorithm
DR	Demand response
DSO	Distribution system operator
ESS	Energy storage system
FR	Frequency regulation
Hetero-ESS	Heterogeneous energy storage system
IAC	Inverter air conditioner
kW	Kilo Watt
RES	Renewable energy source
TES	Thermal battery storage

Set

\mathcal{E}_1	Set of edges for the graph of ESS group
\mathcal{E}_2	Set of edges for the graph of IAC group
\mathcal{I}	Set of IACs
\mathcal{J}	Set of ESSs
\mathcal{T}	Set of time slots
\mathcal{V}_1	Set of vertices for the graph of ESS group
\mathcal{V}_2	Set of vertices for the graph of IAC group

Parameter

A_I	System matrix of ESSs
A_J	System matrix of IACs
D_1	In-degree matrix of $\mathcal{G}_{\mathcal{I}}$
D_2	In-degree matrix of $\mathcal{G}_{\mathcal{J}}$
L_1	Laplacian matrix of ESS group
L_2	Laplacian matrix of IAC group
δ	The decay factor of IAC group
$\eta_i^{\text{in}}, \eta_i^{\text{out}}$	The charging and discharging energy conversion efficiency of the i -th ESS
γ	The interaction gain of the interaction matrix
$\mathcal{G}_{\mathcal{I}}$	The graph of ESSs
$\mathcal{G}_{\mathcal{J}}$	The graph of IACs
A_1	The adjacent matrix of ESS group
A_2	The adjacent matrix of IAC group
a_{ij}	Element of adjacency matrix
C_j	Equivalent air heat capacity of the j -th room
Cap_i	The energy capacity of the i -th ESS

d_i	The i -th diagonal element of the degree matrix
f_j^{\min}, f_j^{\max}	The lower and upper limitation of the j -th IAC's operating frequency
$g(\Delta f, P_{FR})$	The function to calculate the regulation command to relay nodes
K_g	The control gain of the hetero-ESSs
$k_{j,1}, b_{j,1}$	Coefficient of the j -th IAC's operating power
$k_{j,2}, b_{j,2}$	Coefficient of the j -th IAC's cooling capacity
N	Total number of nodes in the communication network
N_1, N_2	The total number of ESSs and IACs
P_i^c, P_i^d	The charge and discharge power limit of the i -th ESS
$P_{j,\text{baseline}}$	The power baseline of the j -th IAC to maintain a steady indoor temperature with a constant outside temperature
$P_{j,\text{TES}}$	The equivalent power of IAC after subtracting the power baseline
R	The relay matrix to receive the regulation command
R_E	The interaction matrix to transmit information from $\mathcal{G}_{\mathcal{I}}$ to $\mathcal{G}_{\mathcal{J}}$
R_j	Equivalent thermal resistance of the j -th room's envelope
SoC^{\min}, SoC^{\max}	The maximum and minimum value of the state of charge of the ESS
T_j^{set}	The initial set temperature of j -th room
T_j^{\max}, T_j^{\min}	The upper and lower bound of comfort range

Variable

X_I	The state vector of N_I ESSs
X_J	The state vector of N_J IACs
Δf	Local frequency deviation
f_j	Operating frequency of the j -th IAC
P_i	The power of the i -th ESS
P_j	Operating power of the j -th IAC
P_{FR}	Total regulated power in real time
P_{tgt}	Target regulation power sent from DSO
Q_j	Cooling capacity of the j -th IAC
soc_i, p_i	The standardized state of charge and power of the i -th ESS
soc_j, p_j	The standardized state of charge and power of the j -th IAC
T^{out}	Outdoor temperature
T_j^{set}	The initial temperature set-point of IAC
T_j^{in}	Indoor air temperature with the j -th IAC
V	Lyapunov function
x_i, x_j	The standardized state vector of i -th ESS and j -th IAC

I. INTRODUCTION

TO CREATE a low-carbon energy system, renewable energy sources (RESs) have increased rapidly in recent years [1]. However, on one hand, the fluctuation of the

RESs' output with variable environment result in an increased requirement for load-following reserve. On the other hand, frequent weather-related incidents involving RESs have heightened the demand for frequency regulation in the power system (e.g., the accidental shutdown of Hornsea offshore wind farm in U.K. on August 9, 2019 triggered around 1,880 MW power output loss) [2]. Consequently, frequency regulation (FR) is becoming more important [3]. FR is provided by conventional generators on the supply side. As more RESs are connected to the power system, conventional generators are phased out gradually and may soon be insufficient for FR. With the rapid development of information and communication technologies, controlling RESs on the demand side becomes feasible, which is called demand response (DR) [4]. Loads on the demand-side can adjust their operating power to mitigate the frequency deviation when the power imbalance incurs [5]. Additionally, customers can earn financial benefits if they participate in DR [6]. Therefore, this mutually beneficial relationship encourages researchers to shift their focus from the supply side to the demand side [7].

Among the demand-side loads, air conditioners (ACs) are ideal candidates for DR, as they account for approximately 40% of total electricity consumption in summer [8]. Furthermore, the thermal storage capacity of the buildings enables the adjustment of the AC operating power without significantly affecting indoor temperature [9]. In general, ACs can be divided into two categories: fixed-frequency ACs and inverter ACs (IACs) [10]. IACs have been widely considered as promising FR resources for the following two reasons: *i*) IACs can be more flexible by changing the compressor frequency compared to fixed-frequency ACs [11]; *ii*) IACs are taking an increasing proportion in ACs' market due to the higher energy efficiency [12]. Numerous studies have attempted to engage IACs in FR. Hui et al. [13] proposed an equivalent model of IACs with power generators for FR. A hierarchical control framework for using AC to provide primary FR is proposed in [14]. However, these papers either ignore the ramp speed or assume a constant value for both ramp-up and ramp-down constraints, which is inconsistent with the actual behavior of the IACs: *i*) The regulation speed of IACs is slow. *ii*) The ramp-up and ramp-down speeds have significant differences. It takes longer for IACs to ramp up than to ramp down in practice. Therefore, most previous research on IACs may no longer satisfy the requirements of FR [15].

Apart from IACs, energy storage systems (ESSs) are potential regulating resources for their fast response speed [16]. More communities and commercial buildings recently installed small emergency ESSs to ensure a high-quality power supply [17]. Unlike the ESSs on the supply-side with great capacity, the energy and power capacity of ESSs on the demand-side are small [18]. Regulating these ESSs would not have a significant effect on the power system. Some studies propose methods to aggregate and regulate multiple small ESSs as a shared ESS [19]. Ma et al. [20] proposes an hour-ahead optimization strategy for shared ESSs to provide FR service. However, the excessive costs of construction and the large initial investments prevent communities from having small ESSs [21]. Therefore, increasing the total capacity of ESSs may not be the most economical approach.

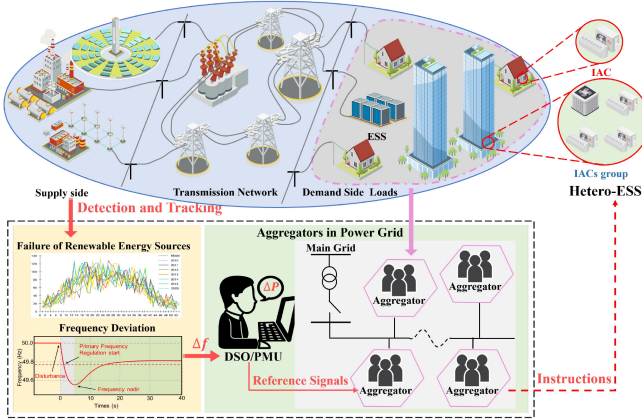


Fig. 1. The control framework of hetero-ESS aggregators to provide FR in power system.

Combining ESSs in the communities with distributed IACs on demand-side can be a feasible solution. The control framework and hetero-ESSs model are shown in Fig. 1. ESSs have fast response speed but small regulation capacities. IACs have huge regulation potential, while the regulation speeds are hard to meet the requirements. The aggregation and regulation of these resources allows for the leveraging of their advantages while mitigating their drawbacks. Some studies proposed coordinated control of different resources to provide high-quality regulation services. In [22], a coordination control of distributed resources is designed under a centralized structure. Zhong et al. [23] proposed a coordinated control strategy for large-scale battery ESSs and traditional FR resources. However, these works are based on a centralized control structure, as shown in Fig. 2(a), which highly demands on the control center and leads to several problems: *i*) As the number of distributed resources increases, the computation burden on the control center rises sharply. *ii*) The communication network of a centralized control structure is vulnerable, once the control center is out of service, the system will be uncontrollable. *iii*) Customers have to share their information with the control center, which is prone to privacy leakage.

As illustrated in Fig. 2(b), distributed control is a more appropriate means of regulating distributed resources on the demand-side: *i*) The nodes under distributed control have certain information processing capabilities, which reduce the computation burden of the control center. *ii*) It does not require full communication access, as every device only communicates with its neighbors or trusted ones, reducing the communication pressure on specific nodes and protecting customers' privacy to a certain extent. Consensus-based distributed control has been the focus of studies. The concept of consensus-based distributed control aims to ensure fair utilization of available devices by facilitating information exchange across sparse communication graph. A consensus integral controller is proposed for the ESSs to synchronize SoC and power with limited information exchange in [24]. A consensus-based control of IACs for frequency regulation in an island microgrid is proposed in [25]. These papers have good regulation performance but take a long time to reach the convergence.

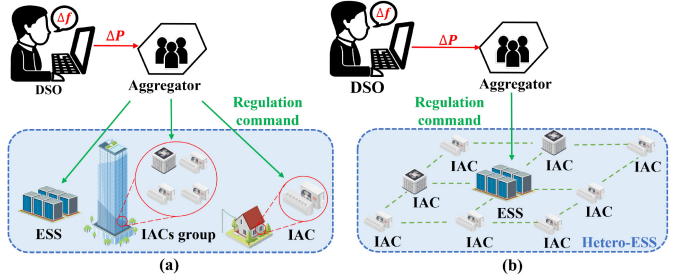


Fig. 2. Control framework of hetero-ESSs aggregator: (a) Centralized control; (b) Distributed coordinated control of ESSs and IACs.

To converge in finite time, a dual consensus-based distributed control approach for multiple ESSs is proposed in [26], which considers the case where generators do not have enough regulation capacity. A distributed finite-time consensus control is proposed for heterogeneous battery ESSs in [27]. A finite-time consensus method for aggregated ESSs is proposed to provide FR in [17]. The methods proposed in these papers can ensure the convergence of the system in finite time but generate a heavy communication burden on communication network. To reduce the communication burden, a distributed event-triggered consensus optimal control method is proposed for ESS in [28]. Information can be passed between two nodes only when the information difference between two nodes reaches the threshold. However, these studies have two limitations: *i*) They do not fully exploit the regulation potential of IACs. The distributed networks have separate control for the IAC and ESS groups, which made the ESS group respond very quickly, while the IAC group act much slower. *ii*) They only focus on the frequency regulation process without considering the ESS recovery process. As a high-quality frequency regulation resource, ESSs need to maintain sufficient capacity to ensure the stability of the power system.

To address the issues above, this paper models distributed IACs as heterogeneous distributed thermal battery storage and then proposes a coordinated control for hetero-ESS as an aggregator. The main contributions are summarized as follows:

- 1) A distributed consensus algorithm (DCA) is designed for hetero-ESS to provide FR under the coordinated framework. The normalized state-space equations of IACs and ESS are modeled for DCA. In contrast to the centralized control strategy, the proposed DCA does not need control center and provides superior scalability, plug-and-play capabilities, and lower communication burden.
- 2) Besides, the proposed DCA takes the short-term regulation ability and long-term regulation flexibility into account. *i*) The widespread distribution of IACs ensures substantial power and energy capacity for the aggregators, while ESSs contribute rapid response and efficient ramp-up speeds. *ii*) The coordinated framework accounts for the energy capacity recovery process of ESS. The aggregator will recharge the energy loss of ESSs, ensuring continuous regulation capability.
- 3) The convergence of the proposed DCA is proved based on the Lyapunov stability theorem. Different physical

characteristics and heterogeneous parameters of ESSs and IACs in the aggregator are taken into consideration.

The remainder of this paper is organized as follows. First, the system framework and models are introduced in Section II. The distributed control algorithm is presented in Section III. Section IV illustrates numerical studies. Section V concludes this paper.

II. DISTRIBUTION SYSTEM MODELLING FOR FREQUENCY REGULATION

A. Coordinated Control Framework of Hetero-ESS

The coordinated control framework of hetero-ESSs for FR is shown in Fig. 1. From the perspective of the supply-side, the output fluctuations of RESs cause the frequency deviation and FR is needed to maintain the stability of power system. Once the frequency deviation exceeds the deadband, the distribution system operator (DSO) or the Phasor Measurement Units (PMU) will send the regulation signals to aggregators on demand-side [29]. On the demand-side, distributed IACs are monitored and regulated as thermal ESSs, and then aggregated with the ESSs in the community as hetero-ESSs. The hetero-ESSs controlled by the local aggregators respond to the regulation command under the control method we proposed.

B. Dynamic Model of ESS

Lithium batteries are a common type of ESS [30]. The state of charge (SoC) is a key parameter to describe the storage level of a Lithium battery [31]. Considering the efficiency of charge/discharge and self-discharge of ESS, the update of SoC is defined as:

$$\dot{SoC}_i(t) = -\sigma SoC_i(t) + \frac{\eta_i}{Cap_i} P_i(t), \forall i \in \mathcal{I}, \forall t \in \mathcal{T}, \quad (1)$$

$$\eta_i(t) = \begin{cases} \eta_i^{\text{in}}, P_i(t) \geq 0 \\ \frac{1}{\eta_i^{\text{out}}}, P_i(t) < 0 \end{cases}, \forall i \in \mathcal{I}, \forall t \in \mathcal{T}, \quad (2)$$

where σ is the rate of energy dissipation due to the self-discharge [32]; η_i is the charging/discharging efficiency of the ESS, which satisfies $0 < \eta_i^{\text{in}} < 1$ and $0 < \eta_i^{\text{out}} < 1$; Cap_i is the maximum energy storage capacity of the ESS; $P_i(t)$ is the actual power of the ESS; \mathcal{I} is the set of ESSs. Because of the physical limitations, $P_i(t)$ is constrained by:

$$-P_i^d \leq P_i(t) \leq P_i^c, \forall i \in \mathcal{I}, \forall t \in \mathcal{T}, \quad (3)$$

where P_i^d and P_i^c are the maximum discharging/charging power of the ESS, respectively. To achieve fair utilization of available regulation resources, this paper applies a consensus-based DCA to control the ESS group. The fundamental mechanism of this consensus-based approach involves information exchange among nodes via a sparse communication network. Typically, consensus control leverages the state of nodes as the exchanged information, with each node's state falling within the same interval. However, owing to the parameter heterogeneity among ESSs, variations exist in the maximum power output of each ESS. Consequently, utilizing the actual power P_i of an ESS as the state for information exchange in consensus control is not feasible. To address this limitation,

we introduce standardized operating power p_i and standardized State of Charge soc_i for the i -th ESS as follows:

$$P_i^{\max} = \begin{cases} P_i^c, P_i(t) \geq 0 \\ P_i^d, P_i(t) < 0 \end{cases}, \forall i \in \mathcal{I}, \forall t \in \mathcal{T}, \quad (4)$$

$$p_i(t) = \frac{P_i(t)}{P_i^{\max}}, \forall i \in \mathcal{I}, \forall t \in \mathcal{T}, \quad (5)$$

$$soc_i(t) = \frac{SoC_i(t) - SoC_i^{\min}}{SoC_i^{\max} - SoC_i^{\min}}, \forall i \in \mathcal{I}, \forall t \in \mathcal{T}, \quad (6)$$

where SoC_i^{\max} and SoC_i^{\min} are the upper and lower SoC boundaries of i -th ESS set by the owner according to their demands, respectively. These standardized values ensure that $soc_i(t)$ lies within the interval $[0, 1]$ and $p_i(t)$ falls within $[-1, 1]$. As a result, p_i and soc_i can serve as the state variables for information exchange among nodes. Specifically, we define the state vector of the i -th ESS as $x_i = \begin{bmatrix} soc_i(t) \\ p_i(t) \end{bmatrix}$. Combining (1)-(6), we can derive the state space model of ESS as:

$$\dot{x}_i(t) = A_i x_i(t) + B_i u_i, \forall i \in \mathcal{I}, \forall t \in \mathcal{T} \quad (7)$$

where $A_i = \begin{bmatrix} a_{11,i} & a_{12,i} \\ 0 & 0 \end{bmatrix}$ and $B_i = \begin{bmatrix} 0 \\ 1 \end{bmatrix}$ are the system and the input matrices, respectively; u_i is the input vector, which will be introduced in Section III-A. The elements $a_{11,i}$ and $a_{12,i}$ in A_i can be respectively expressed as:

$$a_{11,i} = -\sigma, a_{12,i} = \frac{\eta_i \cdot P_i^{\max}}{Cap_i (SoC_i^{\max} - SoC_i^{\min})}, \forall i \in \mathcal{I}. \quad (8)$$

Generally, the owners of ESSs would not change the upper and lower SOC limit frequently. Therefore, we assume that SoC_i^{\max} and SoC_i^{\min} are constant during FR. As a result, $a_{11,i}$ and $a_{12,i}$ are a constant value during the FR for the i -th ESS.

C. Thermal Energy Storage Modeling of IACs

1) *Thermodynamic Model of IAC*: Generally, the power consumption of IACs is related to the ambient temperature and thermal parameters of buildings. In most papers, the equivalent thermodynamic model of a building can be described as in [13]:

$$C_j \frac{\partial T_j^{\text{in}}(t)}{\partial t} = \frac{T_j^{\text{out}}(t) - T_j^{\text{in}}(t)}{R_j} - Q_j(t), \forall j \in \mathcal{J}, \forall t \in \mathcal{T}, \quad (9)$$

where C_j and R_j are the heating capacity and heat resistance of the j -th building, respectively; T_j^{out} is the ambient temperature outside the building at time t ; $Q_j(t)$ is the cooling capacity of the j -th IAC; \mathcal{J} is the set of IACs.

The main power consumption of an IAC in cooling mode comes from the compressor, which can be flexibly adjusted according to the cooling capacity requirement [33]. Generally, the operating power P_j and the cooling power Q_j are both proportional to the operating frequency of compressor f_j , which can be respectively described as:

$$\begin{cases} P_j(t) = k_{j,1} f_j(t) + b_{j,1} \\ Q_j(t) = k_{j,2} f_j(t) + b_{j,2} \end{cases}, \forall j \in \mathcal{J}, \forall t \in \mathcal{T}, \quad (10)$$

$$f_j^{\min} \leq f_j(t) \leq f_j^{\max}$$

where $k_{j,1}$ and $b_{j,1}$ are the coefficients of the j -th IAC's operating power; $k_{j,2}$ and $b_{j,2}$ are the coefficients of the j -th IAC's cooling capacity; f_j^{\min} and f_j^{\max} are the physical constraints of the compressor.

2) *TES Model of IAC in Alignment With ESS Model:* Typically, customers grant aggregators the authority to adjust the power of IACs within a certain range of temperature variations to ensure the comfort of the user [34]. To prevent excessive regulation that could lead to significant temperature deviations for individual customers, this paper proposed a consensus-based DCA to control the IAC group. Due to the heterogeneity of IACs, utilizing the actual power of IAC as the state for information exchange in consensus control is not feasible. Besides, for seamless information exchange between the IAC group and the ESS group, it is essential to unify the state of both group within the value domain. Therefore, we introduce the TES model for IAC [9].

The main difference between an ESS and an IAC in electrical features is that an ESS is capable of charging and discharging, whereas an IAC cannot discharge. In the summer cooling scenario, we define the power necessary for an IAC to maintain the indoor temperature at the set point as the power baseline $P_{j,\text{baseline}}$, which can be derived from (9)-(10) as follows:

$$P_{j,\text{baseline}} = \frac{k_{j,1}(T_j^{\text{out}} - T_j^{\text{set}})}{k_{j,2}R_j} + \frac{k_{j,2}l_{j,1} - k_{j,1}l_{j,2}}{k_{j,2}}, \quad \forall j \in \mathcal{J}, \quad (11)$$

where T_j^{set} is the temperature set by the customers. If operating power consumption falls below $P_{j,\text{baseline}}$, the resulting indoor temperature will be higher than T_j^{set} in steady state. Conversely, if the power exceeds $P_{j,\text{baseline}}$, the indoor temperature will be lower than T_j^{set} in steady state. We assume T_j^{out} and T_j^{set} vary little and can be treated as constant for the duration. Meanwhile, the operating coefficients $k_{j,1}$, $b_{j,1}$, $k_{j,2}$ and $b_{j,2}$ in (10) can be treated as fixed values within the comfort range [9]. Therefore, $P_{j,\text{baseline}}$ can be considered as a fixed value.

Without stopping the compressor, the operating power of IAC is limited by the upper and lower bounds of the compressor's frequency. We define the equivalent TES power $P_{j,\text{TES}}(t)$ as the deviation of the operating power $P_j(t)$ from $P_{j,\text{baseline}}$, which can be expressed as:

$$P_{j,\text{TES}}(t) = P_j(t) - P_{j,\text{baseline}}, \quad \forall j \in \mathcal{J}, \forall t \in \mathcal{T}, \quad (12)$$

$$\begin{cases} P_j^c = k_{j,1}f^{\max} + b_{j,1} - P_{j,\text{baseline}} \\ P_j^d = P_{j,\text{baseline}} - k_{j,1}f^{\min} - b_{j,1} \end{cases}, \quad \forall j \in \mathcal{J}, \quad (13)$$

where P_j^c and P_j^d are the equivalent maximum charging and discharging power of the TES model for IACs, respectively. In this case, $P_{j,\text{TES}}(t)$ can be positive or negative. The practical meaning of $P_{j,\text{TES}}(t)$ is the power of the deviation from the power required to maintain $T_j^{\text{in}} = T_j^{\text{set}}$, and the greater the absolute value of $P_{j,\text{TES}}(t)$, the greater the temperature deviation in steady state when other parameters remain unchanged.

However, $P_{j,\text{TES}}(t)$ cannot be taken as the exchanged information in consensus control. We define the standardized form of $P_{j,\text{TES}}$ as follow:

$$P_j^{\max} = \begin{cases} P_j^c, P_j(t) \geq 0 \\ P_j^d, P_j(t) < 0 \end{cases}, \quad \forall j \in \mathcal{J}, \forall t \in \mathcal{T}, \quad (14)$$

$$p_j(t) = \frac{P_{j,\text{TES}}(t)}{P_j^{\max}}, \quad p_j(t) \in [-1, 1], \quad \forall j \in \mathcal{J}, \forall t \in \mathcal{T}, \quad (15)$$

Generally, the indoor temperature is constrained within the set values to guarantee customers' comfort, i.e., $T_j^{\text{in}} \in [T_j^{\min}, T_j^{\max}]$. The energy capacity stored in buildings depends on $\Delta T = T_j^{\max} - T_j^{\min}$. The energy stored in the buildings is maximum when the indoor temperature is T^{\min} and lowest when T^{\max} . Similar to the definition of SoC for ESS, we can define the SoC of IAC as:

$$soc_j(t) = \frac{T_j^{\max} - T_j(t)}{T_j^{\max} - T_j^{\min}}, \quad \forall j \in \mathcal{J}, \forall t \in \mathcal{T}, \quad (16)$$

where $soc_j(t)$ is the SoC of the j -th IAC, which satisfies $soc_j(t) \in [0, 1]$.

Derived from (9)-(15), the TES model for IACs can be presented in a state space model as:

$$\dot{x}_j(t) = A_j x_j(t) + B u_j, \quad \forall j \in \mathcal{J}, \forall t \in \mathcal{T}, \quad (17)$$

where $x_j = \begin{bmatrix} soc_j(t) \\ p_j(t) \end{bmatrix}$ and $A_j = \begin{bmatrix} a_{11,j} & a_{12,j} \\ 0 & 0 \end{bmatrix}$ are the state vector and the system matrix of the j -th IAC, respectively; u_j is the input vector of the j -th IAC; $a_{11,j}$ and $a_{12,j}$ are the lumped parameters of the j -th IAC, which can be respectively expressed as:

$$a_{11,j} = -\frac{1}{C_j R_j}, \quad a_{12,j} = \frac{k_{j,2} \cdot P_j^{\max}}{C_j k_{j,1} (T_j^{\max} - T_j^{\min})}, \quad \forall j \in \mathcal{J}, \quad (18)$$

which are constant values for the j -th IAC.

III. DISTRIBUTED CONTROL STRATEGY DESIGN AND CONVERGENCE ANALYSIS

A. State Space of Hetero-ESS

Since the IAC's own control program can restore the IAC itself to the initial state after regulation, this study only focuses on the recovery process of the ESSs during the FR. The recovery of ESS means the SoC of ESS at steady state is expected to recover to the initial SoC before FR to ensure sufficient regulation capacity. Therefore, the convergence objects of ESS group in steady state can be expressed as:

$$SoC_i(t) = SoC_i(0), \quad \forall i \in \mathcal{I}, t \rightarrow \infty, \quad (19a)$$

$$P_i(t) = P_i(0), \quad \forall i \in \mathcal{I}, t \rightarrow \infty, \quad (19b)$$

where $SoC_i(0)$ is the initial SoC of the i -th ESS; $P_i(0)$ is the initial power of the i -th ESS.

As x_i in (7) and x_j (17) share the same value domain and both represent the state of a node, nodes within two distinct groups can exchange information across a communication network, which can be represented as the interaction matrix R_E . Considering the heterogeneity of the parameters, x_i and

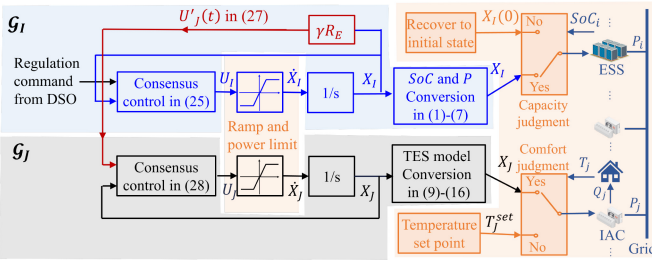


Fig. 3. Control flow chart of the distributed control algorithm.

x_j should satisfy the following equations during FR under the control of consensus-based DCA:

$$p_1(t) = \dots = p_i(t), \forall i \in \mathcal{I}, \quad (20a)$$

$$p_1(t) = \dots = p_j(t), \forall j \in \mathcal{J}, \quad (20b)$$

1) *The Control Input for ESS Group*: We define the input vector of ESS group in (7) as:

$$\dot{\mathbf{U}}_I(t) = -(L_I + \delta I_{N_I}) \otimes K_g \mathbf{X}_I(t), \forall t \in \mathcal{T}, \quad (21)$$

where $\mathbf{X}_I = [x_1^T, \dots, x_i^T]^T$ is the state vector of ESS group; $L_I = \frac{1}{d_i^{\max}} \cdot L_1$ is the control matrix; L_1 is the Laplacian matrix of $\mathcal{G}_{\mathcal{I}}$, which is strongly connected; d_i^{\max} is the maximum out-degree of node in the graph $\mathcal{G}_{\mathcal{I}}$; notation \otimes means the Kronecker-product and its definition can be found in Appendix B; $K_g = [\alpha, \beta]_{1 \times 2}$ is control gain of the input vector; δ is the decay factor, which ensures the convergence target (19b).

Derived from (7) and (21), the state space of ESSs can be represented as:

$$\dot{\mathbf{X}}_I(t) = (\mathbf{A}_I - (L_I + \delta I_{N_I}) \otimes (BK_g)) \mathbf{X}_I, \forall t \in \mathcal{T}. \quad (22)$$

where $\mathbf{A}_I = \text{diag}([A_1, \dots, A_i])$ is the system matrix; I_N is the $N \times N$ identity matrix.

As shown in Fig. 3, DSO or PMU sends the regulation command to ESSs, which work as relay nodes in the communication graph. The regulation command can be a function of the local frequency deviation Δf collected from PMU [29] or a target regulation power P_{tgt} from DSO, which can be represented as $g(\Delta f, P_{FR})$. Assuming the i -th ESS receives the regulation command, the dynamic state of the relay nodes can also be represented as:

$$\begin{aligned} \dot{\mathbf{X}}_I(t) &= (\mathbf{A}_I - (L_I + \delta I_{N_I}) \otimes (BK_g)) \mathbf{X}_I(t) \\ &\quad + R \otimes B \cdot g(\Delta f, P_{FR}), \forall t \in \mathcal{T}, \end{aligned} \quad (23)$$

where $R \in \mathbb{R}^{N_1 \times 1}$ is the relay matrix of ESS consisting of 0 and 1, and 1 represents that the i -th ESS can receive the regulation command.

2) *The Control Input for IAC Group*: The control input of the IAC group $\mathbf{U}_J(t)$ is designed as:

$$\mathbf{U}_J(t) = -(L_J \otimes (BK_g) \mathbf{X}_J(t) + \mathbf{U}'_J(t)), \forall t \in \mathcal{T}, \quad (24)$$

where $\mathbf{X}_J = [x_1^T, \dots, x_j^T]^T$ is the state vector of IAC group, $L_J = \frac{1}{d_j^{\max}} \cdot L_2$ is the control matrix and L_2 is the Laplacian matrix of $\mathcal{G}_{\mathcal{J}}$, which is a strongly connected graph; d_j^{\max} is the maximum out-degree of node in the graph $\mathcal{G}_{\mathcal{J}}$;

$\mathbf{U}'_J(t)$ is the interaction control input introduced from $\mathcal{G}_{\mathcal{I}}$ to achieve information exchange under consensus control. $\mathbf{U}'_J(t)$ is designed as:

$$\mathbf{U}'_J(t) = \gamma R_E \otimes (BK_g) \mathbf{X}_I(t), \forall t \in \mathcal{T}, \quad (25)$$

where γ and $R_E \in \mathbb{R}^{N_2 \times N_1}$ are the interaction gain and the interaction matrix of the hetero-ESSs, respectively.

The value of γ determines the compensation speed of the ESSs in the recovery process. R_E consists of 0 and 1, where 1 in j th row and i th column represents that j -th IAC and i -th ESS are adjacent in the communication graph. From (17) and (24), the state space of IACs can be derived as:

$$\begin{aligned} \dot{\mathbf{X}}_J(t) &= (\mathbf{A}_J - L_J \otimes (BK_g)) \mathbf{X}_J(t) \\ &\quad - \gamma R_E \otimes (BK_g) \mathbf{X}_I(t), \forall t \in \mathcal{T}. \end{aligned} \quad (26)$$

where $\mathbf{A}_J = \text{diag}([A_1, \dots, A_j])$ is the system matrix of IAC group. Combining (22) and (26), the state space of the hetero-ESSs under the control of proposed DCA with considering the regulation command is as follows:

$$\begin{bmatrix} \dot{\mathbf{X}}_I(t) \\ \dot{\mathbf{X}}_J(t) \end{bmatrix} = \left(\begin{bmatrix} \mathbf{A}_I & 0 \\ 0 & \mathbf{A}_J \end{bmatrix} - \begin{bmatrix} L_I + \delta I_{N_I} & 0 \\ \gamma R_E & L_J \end{bmatrix} \otimes (BK_g) \right) \begin{bmatrix} \mathbf{X}_I(t) \\ \mathbf{X}_J(t) \end{bmatrix}, \forall t \in \mathcal{T}. \quad (27)$$

B. Convergence Analysis of the Proposed Algorithm

The convergence of the system is a major concern in distributed consensus control. To verify the stability of the system, the constraints of K_g should be determined. In this section, we prove the hetero-ESSs in (27) are asymptotically stable under the control of the proposed DCA with Lyapunov theorem.

Theorem 1: The proposed control algorithm is Lyapunov asymptotically stable when L_1 is the Laplacian matrix of a strongly connected graph and $K_g = \theta_1 B^T U$, where the positive diagonal matrix U satisfies the following inequality:

$$\bar{U} \bar{A}_i + \bar{A}_i^T U - \theta_1 U B B^T U + \theta_2 U_1 \leq 0, \quad (28)$$

where $U_1 = \text{diag}([1, 1/\theta_2])$ is a positive diagonal matrix; and $0 \leq \theta_1 \leq \frac{\lambda_2^2}{\lambda_{N_1}}$ and $\theta_2 \geq \lambda_{N_1}$, respectively; \bar{A}_i has the biggest nonzero eigenvalue in A_I . Symbols λ_{N_1} and λ_2 are the maximum and second smallest eigenvalues of Laplacian matrix L , respectively [28].

Proof: For hetero-ESS, the proof has two parts. We first prove that the ESS group converges and recovers to the initial state at steady state in *Part I*. In *Part II*, we prove the IAC group converges at steady state given a similar Lyapunov function. We take the parameters of ESS group for example. In fact, the proof procedures for ESS and IAC groups are similar. ■

Part I: In the proof, the regulation command received by the relay nodes can be omitted, since we can prove the system is stable if the system can converge from any initial state [33]. Therefore, the impact of the regulation command and its effect on the relay node are neglected. We choose the Lyapunov function candidate for ESS group:

$$V_1(t) = \frac{1}{2} \mathbf{X}_I^T(t) (L_I \otimes U) \mathbf{X}_I(t) \geq 0, \quad (29)$$

where $V_1(t) \geq 0$ obviously satisfies the first requirement of Lyapunov function. If the candidate for the Lyapunov function satisfies $\dot{V}_1(t) \leq 0$, the system is asymptotically stable. After substituting $\dot{X}_I(t)$ into $\dot{V}_1(t)$, we derived:

$$\begin{aligned} \dot{V}_1(t) &= \frac{1}{2}X_I^T(t)\left\{(L_1 \otimes U)(A_I - (L_I + \delta I_{N_1}) \otimes (BK_g))\right. \\ &\quad \left.+ (A_I - BK_g \otimes (L_I + \delta I_{N_1}))^T(L_1 \otimes U)\right\}X_I(t) \\ &\leq \frac{1}{2}X_I^T(t)\left\{(L_1 \otimes U)(A_I - L_I \otimes (BK_g))\right. \\ &\quad \left.+ (A_I - BK_g \otimes L_I)^T(L_1 \otimes U)\right\}X_I(t) \\ &\leq \frac{1}{2}X_I^T(t)\left\{(L_1 \otimes U)(I_{N_1} \otimes \bar{A}_I - L_I \otimes (BK_g))\right. \\ &\quad \left.+ (I_{N_1} \otimes \bar{A}_I - BK_g \otimes L_I)^T(L_1 \otimes U)\right\}X_I(t) \\ &= \frac{1}{2}X_I^T(t)\left\{(L_1 \otimes (U\bar{A}_I + \bar{A}_I^T U) - mL_1^2 \otimes UBB^T U)\right\}X_I(t). \end{aligned} \quad (30)$$

Denote $\tilde{A} = \frac{U\bar{A}_I + \bar{A}_I^T U}{2}$, $\tilde{B} = UBB^T U$. Then denote the eigenvalue of Laplacian matrix L_1 as $0 = \lambda_1 < \lambda_2 \leq \dots \leq \lambda_{N_1}$; $\Lambda = \text{diag}([\lambda_1, \dots, \lambda_{N_1}])$. Let $Y(t) = (Q^T \otimes I_2)X_I(t)$, Q is the orthogonal matrix and it always guarantees:

$$Q^T L Q = Q^{-1} L Q = \Lambda = \text{diag}(\lambda_1, \lambda_2, \dots, \lambda_{N_1}). \quad (31)$$

After the space transformation, it derives:

$$\begin{aligned} \dot{V}_1(t) &\leq X_I^T(t)(L_1 \otimes \tilde{A} - mL_1^2 \otimes \tilde{B})X_I(t) \\ &= Y^T(t)(Q^T L_1 Q \otimes \tilde{A} - mQ^T L_1^2 Q \otimes \tilde{B})Y(t) \\ &\leq Y^T(t)(\Lambda \otimes \tilde{A} - m\Lambda^2 \otimes \tilde{B})Y(t) \\ &= \sum_{i=1}^{N_1} \lambda_i Y^T(t)(\tilde{A} - m\lambda_i \tilde{B})Y(t). \end{aligned} \quad (32)$$

Given $0 \leq \theta_1 \leq \frac{m\lambda_2^2}{\lambda_{N_1}}$ and $\theta_2 \geq \lambda_{N_1}$, it derives:

$$\begin{aligned} \dot{V}_1(t) &\leq \sum_{i=1}^{N_1} \lambda_i Y^T(t)(\tilde{A} - \theta_1 \tilde{B})Y(t) \\ &\leq \sum_{i=1}^{N_1} \lambda_i Y^T(t)(-\theta_2 U_1)Y(t) \\ &\leq -\sum_{i=1}^{N_1} \lambda_i \lambda_{N_1} Y^T(t)U_1 Y(t) \leq 0. \end{aligned} \quad (33)$$

Hence, we prove that $\dot{V}_1(t) \leq 0$ and the system is asymptotically stable as long as the feedback control gain $K_g = \theta_1 B^T U$ and U satisfy the inequality (28).

Part II: Similar to the proof of ESS group, $U_J'(t)$ can be omitted, since we can prove the system is stable if the system can converge from any initial state. We choose the Lyapunov function candidate for IAC group:

$$V_2(t) = \frac{1}{2}X_J^T(t)(L_J \otimes U)X_J(t) \geq 0, \quad (34)$$

¹When L_1 is the Laplacian matrix of a strongly connected graph, it satisfies $\lambda_2 > \lambda_1 = 0$, $\lambda_{N_1} \geq d_i^{\max} + 1$ [35].

TABLE I
PARAMETERS OF ESSS, ACs, AND CORRESPONDING ROOMS

Symbols	Parameters	Distributions ¹ /Values	Units
η^{in}	ESS charge coefficients	$\mathcal{U}(0.93, 0.95)$	-
η^{out}	ESS discharge coefficients	$\mathcal{U}(0.93, 0.95)$	-
σ	ESS self-discharge rate	$\mathcal{U}(0.0001, 0.0003)$	per day
Cap	ESS energy capacity	$\mathcal{U}(30, 40)$	kWh
P^c/P^d	ESS maximum operating power	$\mathcal{U}(30, 40)$	kW
ΔSoC	ESS SoC range ²	$\mathcal{U}(0.4, 0.6)$	kW
k_1	IAC operation coefficients	$\mathcal{U}(0.0285, 0.0315)$	kW/Hz
b_1	IAC operation coefficients	$\mathcal{U}(-0.42, -0.38)$	kW
k_2	IAC cooling coefficients	$\mathcal{U}(0.057, 0.063)$	kW/Hz
b_2	IAC cooling coefficients	$\mathcal{U}(-0.315, -0.285)$	kW
f^{\min}	Lower limitation of IAC operating frequency	$\mathcal{U}(10, 30)$	Hz
f^{\max}	Upper limitation of IAC operating frequency	$\mathcal{U}(130, 150)$	Hz
R	Equivalent thermal resistance	$\mathcal{U}(1.9, 2.1)$	°C/kW
C	Equivalent air heat capacity	$\mathcal{N}(390, 78^2)$	kJ/°C
T^{\max}	Upper bound of comfort range	$\mathcal{U}(26, 27)$	°C
T^{\min}	Lower bound of comfort range	$\mathcal{U}(21, 22)$	°C
T^{\set}	Initial indoor temperature	$\mathcal{U}(24, 25)$	°C
T^{\out}	Outdoor temperature	32	°C

¹ \mathcal{U} denotes uniform distributions, and \mathcal{N} denotes normal distributions.

² $\Delta SoC_i = SoC_i^{\max} - SoC_i^{\min}$.

The proof derivations for $V_1(t)$ and $V_2(t)$ are similar, which will not be repeated in the paper.

IV. CASE STUDIES

In this section, the performance of the aggregator under the control algorithm (27) is tested. We assume that a community with ESSs and 32 buildings is controlled as an aggregator to provide FR. Distributed IACs among the 32 buildings are divided into four groups to coordinate with ESSs in turn for providing FR. The heterogeneous parameters of the ESS, IACs, corresponding rooms' equivalent thermal models and their initial states are shown in Table I. The update frequency in simulation is set as 0.05s, which is feasible based on the current communication technology.

In the case studies, MATLAB R2022b and Simulinks are the simulation environments. Intel Core i7-11700 is the CPU model and its frequency is 2.50 GHz. The outdoor temperature is assumed as fixed value during FR. In the simulation, we take 4 comparison cases as the benchmark: the aggregator under centralized control in Fig. 2(a), the aggregator under the conventional DCA in [33], the aggregator under the conventional DCA without IACs, and the aggregator under the conventional DCA without ESSs.

A. Analysis of the Proposed DCA's Regulation Performance in Short-Term When Receiving Regulation Command From DSO

In this case, the aggregator is assumed to respond immediately to the decomposed regulation command from the DSO, which contains both the target regulation power P_{tgt} and the duration time for FR. Then the aggregator needs to achieve the regulation requirement under the proposed DCA. The regulation command

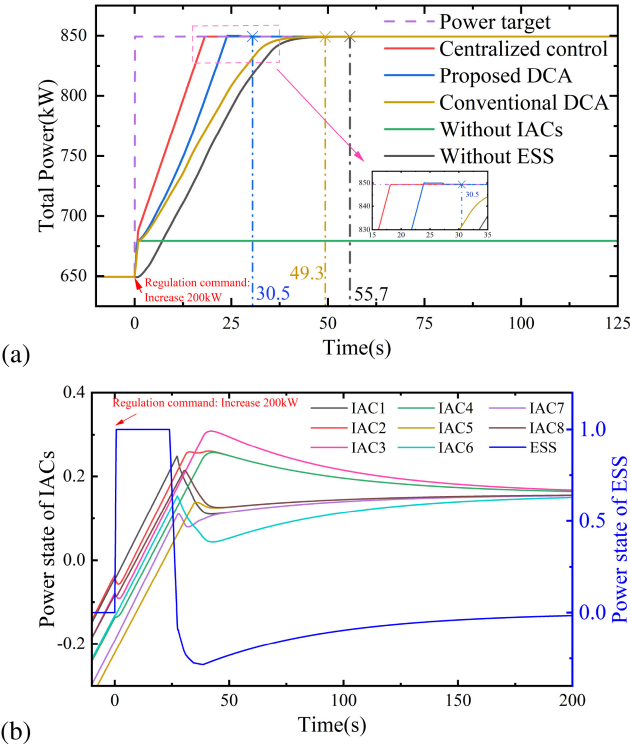


Fig. 4. The regulation performance after receiving the regulation command to increase 200kW: (a) the total power of the aggregator; (b) The power state of the aggregator.

function is defined as $g(P_{FR}) = \theta(P_{tgt} - P_{FR})$, where $\theta = 0.1$ is the control coefficient of the relay node.

For other parameters in this case, the control gain is set as $K_g = [-10, 0.15]$; the decay factor is $\delta = 0.01$; the interaction gain is $\gamma = 0.2$.

The simulation results of upward regulation are shown in Fig. 4(a) and Fig. 4(b). The aggregator successfully achieves the upward regulation command within a response time of $T_R = 30.5$ s under the proposed DCA. Compared with centralized control mechanisms, the proposed DCA has a slight decrease in the response speed and regulation time but maintains sufficient speed. When evaluated against conventional DCA and aggregator without ESS or IAC, the response speed and regulation time of the proposed DCA are better than those of the control methodologies.

The sudden power increase depicted in Fig. 4(a) is due to the ESS swiftly ramping up and reaching the rated power shortly after receiving the regulation command. The magnified view in Fig. 4(a) reveals that the total power provided by the aggregator has a minor fluctuation and marginally exceeds the target power P_{tgt} . This occurrence can be attributed to the progressive replacement of power between ESSs and IACs, which allows the ESS power to recover to the initial value before FR, guaranteeing that ESS has adequate capacity.

The state dynamics of hetero-ESSs is depicted in Fig. 4(b). The figure illustrates that ESS ramps up fast and reach the rated power soon after receiving reference command. Then IACs respond instantaneously and increase the power under ramping up limitation.

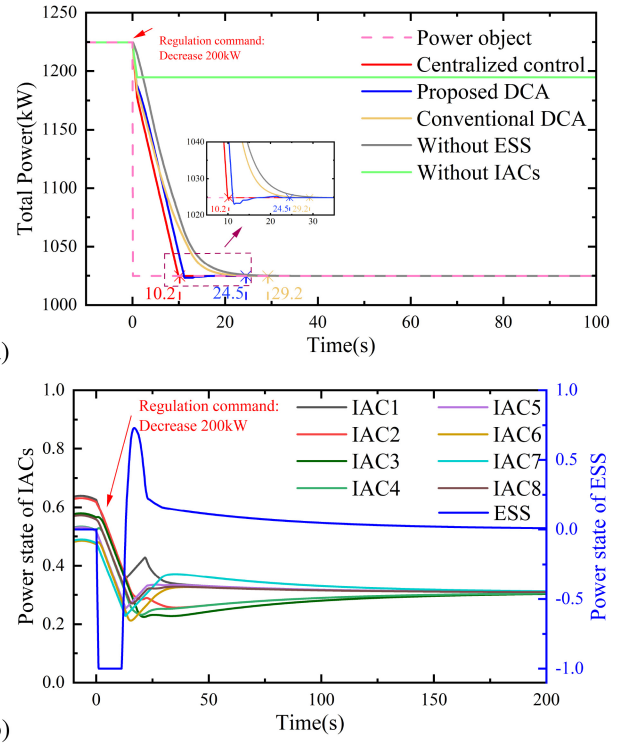


Fig. 5. The regulation performance after receiving the regulation command to decrease 200kW: (a) the total power of the aggregator; (b) The power state of the aggregator.

As the cumulative power provided by the system approaches the required regulation capacity, the power state of the ESS will decrease. Finally, IACs' states achieve consensus and ESS's state stop fluctuating around zero shortly after the hetero-ESSs reach target regulation capacity. During the regulation process, IACs increase power at their maximum ramping speed. The interaction matrix enables rapid adjustments of the ESS and IACs power states without significantly altering the total power, which accelerates the convergence speed of the system. Therefore, the proposed DCA converges faster in contrast to the conventional DCA.

The downward regulation to decrease 200kW is illustrated in Fig. 5(a) and Fig. 5(b). From the magnified view in Fig. 5, the hetero-ESSs provide the required regulation capacity and stop fluctuation within $T_R = 24.5$ s, meeting the FR requirements. The regulation speed of the proposed DCA is slightly slower than the centralized control while faster than the conventional DCA and the aggregation without ESS and IAC. Fig. 5 depicts the power state of the hetero-ESSs. Similar to the upward regulation, the downward regulation consists of three parts: the ESS responding fast with the maximum output; IACs adjusting operating power sequentially; and finally, the power provided by ESS substituted by IACs. Within the aggregation framework, these two resources play a complementary role. The ESSs function as a rapid-response resource, mitigating the fluctuations in the IACs' power output. In contrast, the IACs provide substantial regulation capacity for FR, a feature that the ESS does not have. Furthermore, the information exchanges between the IACs and the ESS in

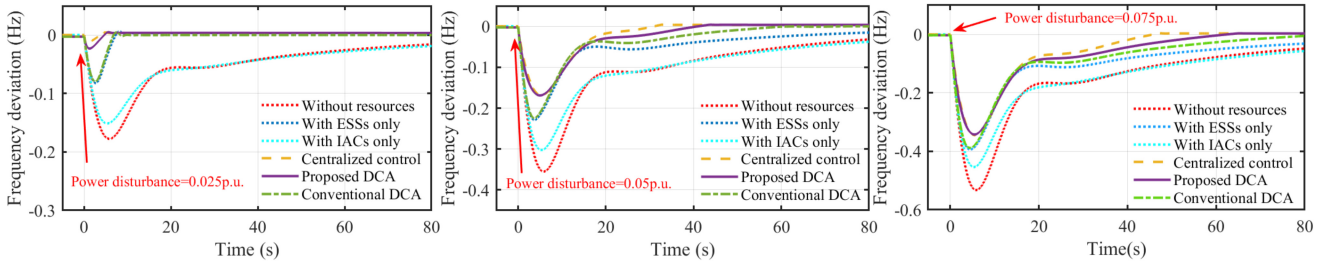


Fig. 6. The system frequency deviations under different control algorithms when the power disturbances of -0.025p.u. , -0.05p.u. and -0.075p.u. occur.

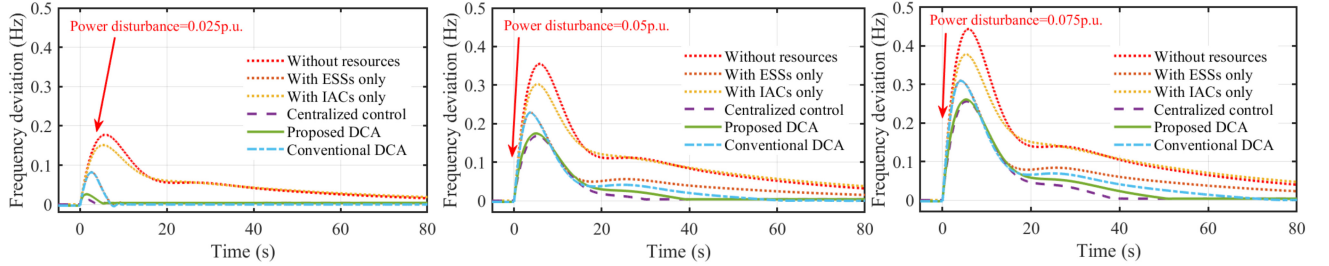


Fig. 7. The system frequency deviations under different control algorithms when the power disturbances of $+0.025\text{p.u.}$, $+0.05\text{p.u.}$ and $+0.075\text{p.u.}$ occur.

TABLE II
ESSS' PARAMETERS IN THE FREQUENCY REGULATION

ESS number	Rated power(MW)	Initial SoC(%)	$\Delta SoC(%)$
ESS1	7.5	55	10
ESS2	2.5	60	30
ESS3	5	75	20
ESS4	5	80	20

the proposed DCA enable the hetero-ESSs to accomplish the above coordination without a control center.

B. Analysis of the Proposed DCA's Regulation Performance Based on the Frequency Deviation From PMU

The FR performance of the proposed DCA requires verification in power system simulation. The total installed capacity of the power system is 800MW with reheat steam and the parameters are shown in detail in APPENDIX C. The nominal frequency of the power system f_n is 50Hz. The system frequency deviation threshold Δf^{thr} is set to 0.05Hz. The total operating power of the IACs is about 10% of the power system capacity. The parameters of ESSs are shown in Table II. The total installed power of the ESSs is about 2.5% of the power system capacity. The installed RESs are assumed to account for 40% of the total installed capacity [36]. For the parameters in this case, the control gain is set as $K_g = [-10, 0.3]$; the decay factor is $\delta = 0.01$; the interaction gain is $\gamma = 0.3$.

Fig. 6 and Fig. 7 illustrate the impact of varying control algorithms on system frequency deviations in response to power disturbances of 0.025 p.u., 0.05 p.u. and 0.075 p.u. When the power disturbance is 0.025p.u., the disturbance is approximately equal to the total installed capacity of the ESSs. Therefore, it can be concluded that the ESSs are capable of balancing disturbances in this scenario. As the

power disturbance increases, relying solely on regulating ESSs becomes insufficient to maintain balance and the frequency nadir f_{nadir} can exceed 0.4Hz, which does not satisfy the frequency requirements of the power system. In such cases, regulating IACs can rectify the frequency nadir f_{nadir} and shorten the settling time of the FR. However, due to the inherent limitations of the IAC's ramping speed, it is challenging for the IACs to balance the disturbance as rapidly as the ESSs. Upon comparing the frequency nadir f_{nadir} and regulation settle time, we observe that the proposed DCA outperforms the conventional DCA for these three disturbances. When compared with centralised control mechanisms, the proposed DCA exhibits a slight decline in response speed, which is nevertheless within an acceptable range. The performance of various strategies in FR under varying power disturbances is summarized in Table III.

Fig. 8 depicts the actual and standardized state of ESSs when the power disturbance is $-0.05pu$. ESSs ramp up fast and reach the rated power soon after receiving the frequency deviation. As the Δf gradually decreases, the output power of the ESSs decreases and finally recover back to the initial state. As with Fig. 9, this figure demonstrates that the SoC of ESSs with disparate initial states can restore to their respective initial values. However, the SoC of ESSs under the conventional DCA will continuously decrease until it reaches the limits, as illustrated in Fig. 10 and Fig. 11. Furthermore, the ESSs must cease working because the SoC of the ESSs has reached the threshold. This rapid shutdown can result in transient power imbalances in the power system.

Fig. 12 depicts the standardized state and the indoor temperature of IACs when power disturbance is -0.05p.u. . During FR, as the power of the IACs decreases, the indoor temperature rises gradually from approximately 25 degrees Celsius to almost the upper limit of the comfort range at the end of the regulation period. Notwithstanding the fact that IACs take a

TABLE III
PERFORMANCE OF DIFFERENT STRATEGIES IN FREQUENCY REGULATION
UNDER VARYING POWER DISTURBANCE

Disturbance	Controller	f_{nadir} (Hz)	Settle time(s)
-0.025p.u.	Centralized control	-0.013	5.8
	Conventional DCA	-0.079	8.55
	Proposed DCA	-0.023	6.6
-0.05p.u.	Centralized control	-0.168	32.85
	Conventional DCA	-0.224	59.20
	Proposed DCA	-0.169	43.90
-0.075p.u.	Centralized control	-0.342	47.50
	Conventional DCA	-0.388	86.10
	Proposed DCA	-0.345	65.20
+0.025p.u.	Centralized control	0.018	5.05
	Conventional DCA	0.081	9.60
	Proposed DCA	0.026	6.4
+0.05p.u.	Centralized control	+0.168	30.15
	Conventional DCA	0.229	60.60
	Proposed DCA	0.175	39.30
+0.075p.u.	Centralized control	0.256	39.15
	Conventional DCA	0.309	77.05
	Proposed DCA	0.261	50.80

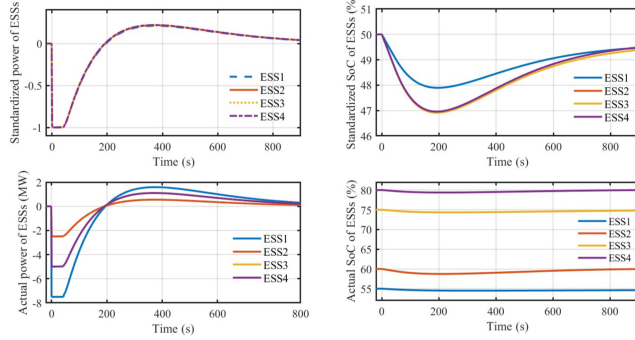


Fig. 8. The standardized and actual state of ESSs under the proposed DCA when power disturbance is -0.05p.u.

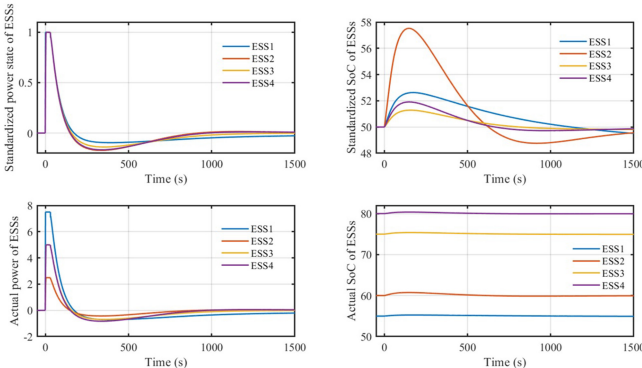


Fig. 9. The standardized and actual state of ESSs under the proposed DCA when power disturbance is +0.05p.u.

significant portion of the system capacity, it is not feasible to regulate them as long-term thermal energy storage.

To achieve long-term regulation, a feasible approach would be to divide the IACs into multiple groups, with each group participating in the regulation in turn. Upon completion of the preceding response, the original control program can

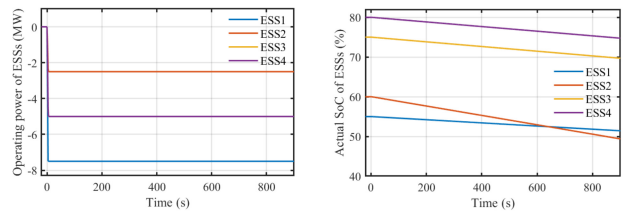


Fig. 10. The power and SoC of ESSs under conventional DCA when power disturbance is -0.05p.u.

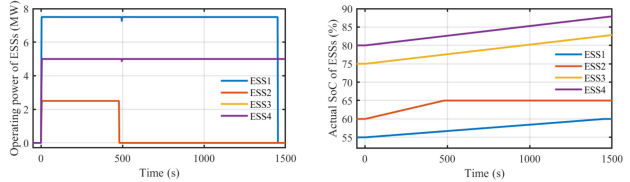


Fig. 11. The power and SoC of ESSs under conventional DCA when power disturbance is +0.05p.u.

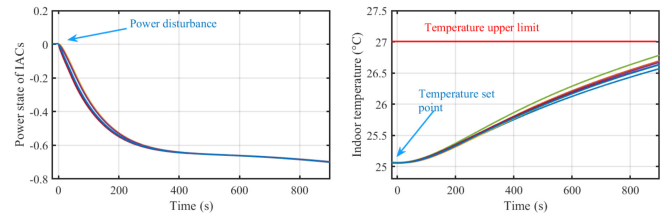


Fig. 12. The standardize state and the indoor temperature of IACs under the proposed DCA when power disturbance is -0.05p.u.

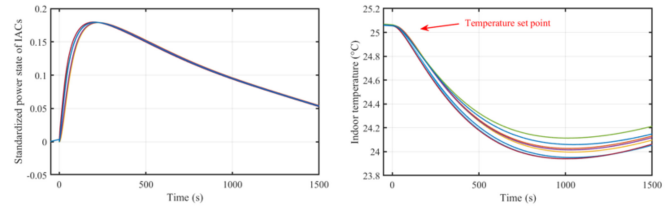


Fig. 13. The standardize state and the indoor temperature of IACs under the proposed DCA when power disturbance is +0.05p.u.

reestablish the IACs to their initial state before the subsequent response. As illustrated in Fig. 14, in response to a disturbance of +0.05p.u., the IAC group provides FR for approximately 1400 seconds before the indoor temperature reaches the upper limit of $T_{max} = 27^{\circ}\text{C}$. Subsequently, the time required for an IAC group to return to the set temperature under the control of its own controller is approximately 4000 seconds, which is approximately three times the duration of the regulation. Therefore, this paper roughly divides IACs into four groups.

Categorizing IACs into groups involves trade-offs. If there are too many groups, the proportion of IACs participating in the response decreases, potentially resulting in poorer regulation performance. On the contrary, having few groups may not allow the IACs to recover to the initial state. Therefore, the exact number of groups should be selected according to the actual system parameters.

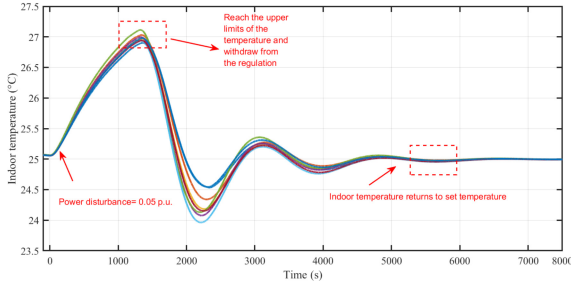


Fig. 14. The recovery process of IAC group under the control of their own controllers after frequency regulation.

V. CONCLUSION

In this paper, we develop the novel model of hetero-ESSs and propose a DCA to control the hetero-ESSs for FR. First, the model of IAC is transformed into an equivalent TES model. Consequently, the regulation capacities of heterogeneous ESSs are standardized. Subsequently, a distributed consensus algorithm is designed for the purpose of controlling hetero-ESSs for FR. The interaction matrix introduced in DCA enables rapid adjustments of the ESS and IACs power states without altering the total power significantly. Within the hetero-ESSs, the energy loss of the ESS can be compensated with a gradual replacement of the power between the ESS and the IACs, thereby ensuring the long-term flexibility of the system. Furthermore, the convergence of the proposed control algorithm is proven based on the Lyapunov stability theorem.

The regulation performance of the proposed DCA for hetero-ESSs is evaluated through numerical simulations. The results demonstrate that the control objects, including the response time and the required regulation capacity, can be achieved successfully when received the regulation command from the DSO. In the short term, the proposed DCA outperforms the conventional DCA under varying disturbances, both in f_{nadir} and the settlement time. The performance of the proposed DCA is not significantly inferior to that of the centralized control, and the distributed system reduces communication and computation overheads. In the long term, the system can provide sustained and continuous response. Consequently, this work may serve as a valuable reference for the utilisation of heterogeneous resources to facilitate frequency regulation in the prospective smart grid.

APPENDIX A

The graph theory is the fundamental of the distributed consensus control strategy. The communication network of a group (ESSs and IACs) can be represented by a graph. In this paper, \mathcal{I}, \mathcal{J} indicates the set of ESSs and IACs, respectively. The total number of ESSs and IACs is assumed as $N = N_1 + N_2$, where N_1, N_2 are the total number of ESSs and IACs, respectively. An undirected graph of ESS group is defined as $\mathcal{G}_{\mathcal{I}} = (\mathcal{V}_1, \mathcal{E}_1, \mathcal{A}_1)$ with a nonempty set of nodes $\mathcal{V}_1 = \{v_1, v_2, \dots, v_{N_1}\}$ and a set of edges $\mathcal{E}_1 \subseteq \mathcal{V}_1 \times \mathcal{V}_1$, and associated adjacency matrix $\mathcal{A}_1 = [a_{ij}]_{N_1 \times N_1}$. As shown in Fig. (15), each node is assigned to an ESS in the DCA, and the edge (v_i, v_j) means that the information can flow from

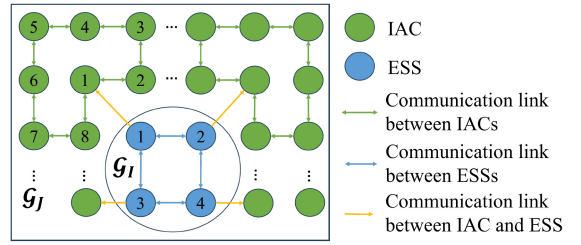


Fig. 15. Communication network of ESSs and IACs.

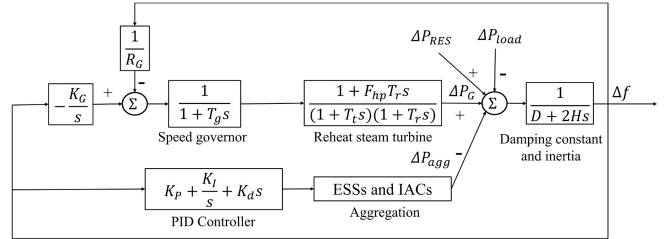


Fig. 16. The power system model considering the frequency regulation from ESSs and IACs.

node i to node j on the graph. The associated adjacency matrix $\mathcal{A}_1 = [a_{ij}]$ of the graph $\mathcal{G}_{\mathcal{I}}$ is defined as:

$$a_{ij} = a_{ji} = \begin{cases} 1, & \text{if } (v_i, v_j) \in \mathcal{E}_1 \\ 0, & \text{otherwise} \end{cases}, \quad (35)$$

which means bidirectional communication exists between two neighbor ESSs [33]. The corresponding Laplacian matrix \mathbf{L}_1 of graph $\mathcal{G}_{\mathcal{I}}$ is defined and calculated by:

$$\mathbf{L}_1 = \mathbf{D}_1 - \mathcal{A}_1, \quad (36)$$

where \mathbf{D}_1 is the out-degree matrix and defined as $\mathbf{D}_1 = \text{diag}(d_1, d_2, \dots, d_{N_1}) \in \mathbb{R}^{N_1 \times N_1}$ with $d_i = \sum_{j \neq i} a_{ij}$. Similarly, we can define the graph of IAC group as $\mathcal{G}_{\mathcal{J}} = (\mathcal{V}_2, \mathcal{E}_2, \mathcal{A}_2)$, $\mathcal{A}_1 = [a_{ij}]_{N_2 \times N_2}$, and the corresponding Laplacian matrix $\mathbf{L}_2 = \mathbf{D}_2 - \mathcal{A}_2$.

APPENDIX B

If A is an $m \times n$ matrix and B is a $p \times q$ matrix, then the Kronecker product $A \otimes B$ is the $mp \times nq$ block matrix:

$$\mathbf{A} \otimes \mathbf{B} = \begin{bmatrix} a_{11}\mathbf{B} & \cdots & a_{1n}\mathbf{B} \\ \vdots & \ddots & \vdots \\ a_{m1}\mathbf{B} & \cdots & a_{mn}\mathbf{B} \end{bmatrix}_{mp \times nq} \quad (37)$$

APPENDIX C

The power system model in the simulation is shown in the Fig. (16). The parameters of the reheat steam synchronous generator are set as follows: the rated capacity S_G is 800MW; the generator inertia H_G is 10s; the time constants of the speed governor T_g , the turbine T_t , and the reheat process T_r are 0.2s, 7s and 0.3s, respectively; the high pressure turbine section F_{hp} is 0.3; the speed droop parameter R_G and the integral gain K_G are 0.05 and 0.5, respectively; the damping constant of the power system D is 1; the inertia of the power system H is 10.

All regulation resources among the comparison cases in Section IV-B use the PID controllers with the following parameters: $K_P = 500$, $K_I = 0.01$ and $K_d = 100$. The regulation command function in (23) is defined as:

$$g(\Delta f) = K_p \Delta f + K_d \frac{d\Delta f}{dt} + K_i \int \Delta f, \quad (38)$$

where Δf is the frequency deviation measured by PMU.

REFERENCES

- [1] X. Yang, Y. Song, G. Wang, and W. Wang, "A comprehensive review on the development of sustainable energy strategy and implementation in China," *IEEE Trans. Sustain. Energy*, vol. 1, no. 2, pp. 57–65, Jul. 2010.
- [2] "Investigation into 9 August 2019 power outage." Aug. 2019. [Online]. Available: <https://www.ofgem.gov.uk/publications-and-updates/investigation-9-august-2019-power-outage>
- [3] Y. Wang, N. Zhang, C. Kang, D. S. Kirschen, J. Yang, and Q. Xia, "Standardized matrix modeling of multiple energy systems," *IEEE Trans. Smart Grid*, vol. 10, no. 1, pp. 257–270, Jan. 2019.
- [4] P. Siano, "Demand response and smart grids—A survey," *Renew. Sustain. Energy Rev.*, vol. 30, pp. 461–478, Feb. 2014.
- [5] P. Palensky and D. Dietrich, "Demand side management: Demand response, intelligent energy systems, and smart loads," *IEEE Trans. Ind. Informat.*, vol. 7, no. 3, pp. 381–388, Aug. 2011.
- [6] J. Wang et al., "Economic benefits of integrating solar-powered heat pumps into a CHP system," *IEEE Trans. Sustain. Energy*, vol. 9, no. 4, pp. 1702–1712, Oct. 2018.
- [7] H. Liu, Z. Hu, Y. Song, J. Wang, and X. Xie, "Vehicle-to-grid control for supplementary frequency regulation considering charging demands," *IEEE Trans. Power Syst.*, vol. 30, no. 6, pp. 3110–3119, Nov. 2015.
- [8] "Air conditioning consumes one third of peak electric consumption in the summer." 2012. [Online]. Available: <https://www.sciencedaily.com>
- [9] M. Song, C. Gao, H. Yan, and J. Yang, "Thermal battery modeling of inverter air conditioning for demand response," *IEEE Trans. Smart Grid*, vol. 9, no. 6, pp. 5522–5534, Nov. 2018.
- [10] N. Mahdavi and J. H. Braslavsky, "Modelling and control of ensembles of variable-speed air conditioning loads for demand response," *IEEE Trans. Smart Grid*, vol. 11, no. 5, pp. 4249–4260, Sep. 2020.
- [11] "What is inverter technology AC." 2018. [Online]. Available: <https://www.bijilibachao.com/air-conditioners/>
- [12] (Int. Energy Agency, Paris, France). *The Future of Cooling*. 2018. [Online]. Available: <https://www.iea.org/reports/the-future-of-cooling>
- [13] H. Hui, Y. Ding, and M. Zheng, "Equivalent modeling of inverter air conditioners for providing frequency regulation service," *IEEE Trans. Ind. Electron.*, vol. 66, no. 2, pp. 1413–1423, Feb. 2019.
- [14] X. Wu, J. He, Y. Xu, J. Lu, N. Lu, and X. Wang, "Hierarchical control of residential HVAC units for primary frequency control," *IEEE Trans. Smart Grid*, vol. 9, no. 4, pp. 3844–3856, Jul. 2018.
- [15] B. Mohandes, M. S. El Moursi, N. Hatziargyriou, and S. El Khatib, "A review of power system flexibility with high penetration of renewables," *IEEE Trans. Power Syst.*, vol. 34, no. 4, pp. 3140–3155, Jul. 2019.
- [16] S. Vazquez, S. M. Lukic, E. Galvan, L. G. Franquelo, and J. M. Carrasco, "Energy storage systems for transport and grid applications," *IEEE Trans. Ind. Electron.*, vol. 57, no. 12, pp. 3881–3895, Dec. 2010.
- [17] Y. Wang et al., "Aggregated energy storage for power system frequency control: A finite-time consensus approach," *IEEE Trans. Smart Grid*, vol. 10, no. 4, pp. 3675–3686, Jul. 2018.
- [18] R. N. Castellano, *Alternative Energy Technologies: Opportunities and markets*. Fontainebleau, France: Archives Contemporaines, 2012.
- [19] B. Zheng, W. Wei, Y. Chen, Q. Wu, and S. Mei, "A peer-to-peer energy trading market embedded with residential shared energy storage units," *Appl. Energy*, vol. 308, Feb. 2022, 118400.
- [20] Y. Ma, Z. Hu, and Y. Song, "Hour-ahead optimization strategy for shared energy storage of renewable energy power stations to provide frequency regulation service," *IEEE Trans. Sustain. Energy*, vol. 13, no. 4, pp. 2331–2342, Oct. 2022.
- [21] A. Evans, V. Strezov, and T. J. Evans, "Assessment of utility energy storage options for increased renewable energy penetration," *Renew. Sustain. Energy Rev.*, vol. 16, no. 6, pp. 4141–4147, 2012.
- [22] N. L. Diaz, A. C. Luna, J. C. Vasquez, and J. M. Guerrero, "Centralized control architecture for coordination of distributed renewable generation and energy storage in islanded AC microgrids," *IEEE Trans. Power Electron.*, vol. 32, no. 7, pp. 5202–5213, Jul. 2017.
- [23] J. Zhong et al., "Coordinated control for large-scale EV charging facilities and energy storage devices participating in frequency regulation," *Appl. Energy*, vol. 123, pp. 253–262, Jun. 2014.
- [24] J. Khazaei and Z. Miao, "Consensus control for energy storage systems," *IEEE Trans. Smart Grid*, vol. 9, no. 4, pp. 3009–3017, Jul. 2018.
- [25] J. Su, H. Zhang, C.-K. Wong, L. Yu, and Z. Tan, "Hierarchical control of inverter air conditioners for frequency regulation service of islanded microgrids with fair power participation," *IEEE Trans. Smart Grid*, vol. 15, no. 5, pp. 4602–4617, Sep. 2024.
- [26] L. Xing et al., "Dual-consensus-based distributed frequency control for multiple energy storage systems," *IEEE Trans. Smart Grid*, vol. 10, no. 6, pp. 6396–6403, Nov. 2019.
- [27] J. Hu and A. Lanzon, "Distributed finite-time consensus control for heterogeneous battery energy storage systems in droop-controlled microgrids," *IEEE Trans. Smart Grid*, vol. 10, no. 5, pp. 4751–4761, Sep. 2019.
- [28] W. Kang, M. Chen, Y. Guan, L. Tang, J. C. Vasquez, and J. M. Guerrero, "Distributed event-triggered optimal control method for heterogeneous energy storage systems in smart grid," *IEEE Trans. Sustain. Energy*, vol. 13, no. 4, pp. 1944–1956, Oct. 2022.
- [29] S. You et al., "Non-invasive identification of inertia distribution change in high renewable systems using distribution level PMU," *IEEE Trans. Power Syst.*, vol. 33, no. 1, pp. 1110–1112, Jan. 2018.
- [30] H. Xing, M. Fu, Z. Lin, and Y. Mou, "Decentralized optimal scheduling for charging and discharging of plug-in electric vehicles in smart grids," *IEEE Trans. Power Syst.*, vol. 31, no. 5, pp. 4118–4127, Sep. 2016.
- [31] K. W. E. Cheng, B. Divakar, H. Wu, K. Ding, and H. F. Ho, "Battery-management system (BMS) and SOC development for electrical vehicles," *IEEE Trans. Veh. Technol.*, vol. 60, no. 1, pp. 76–88, Jan. 2011.
- [32] Y. Wen, W. Li, G. Huang, and X. Liu, "Frequency dynamics constrained unit commitment with battery energy storage," *IEEE Trans. Power Syst.*, vol. 31, no. 6, pp. 5115–5125, Nov. 2016.
- [33] J. Hong, H. Hui, H. Zhang, N. Dai, and Y. Song, "Distributed control of large-scale inverter air conditioners for providing operating reserve based on consensus with nonlinear protocol," *IEEE Internet Things J.*, vol. 9, no. 17, pp. 15847–15857, Sep. 2022.
- [34] H. Hui, Y. Ding, K. Luan, T. Chen, Y. Song, and S. Rahman, "Coupon-based demand response for consumers facing flat-rate retail pricing," *CSEE J. Power Energy Syst.*, early access, Apr. 20, 2023, doi: [10.17775/CSEEPES.2021.05140](https://doi.org/10.17775/CSEEPES.2021.05140).
- [35] R. Merris, "Laplacian matrices of graphs: A survey," *Linear Algebra Appl.*, vols. 197–198, pp. 143–176, Jan./Feb. 1994.
- [36] A. S. Mir and N. Senroy, "Intelligently controlled flywheel storage for enhanced dynamic performance," *IEEE Trans. Sustain. Energy*, vol. 10, no. 4, pp. 2163–2173, Oct. 2019.



Ruiwen Liu (Graduate Student Member, IEEE) received the B.S. degree in mechanical science and engineering from the Huazhong University of Science and Technology, Wuhan, China, in 2022. He is currently pursuing the Ph.D. degree in electrical and computer engineering with the University of Macau, Macau, SAR, China.

His research focuses on control of power system, demand response, and the smart hydrogen energy.



Hongxun Hui (Member, IEEE) received the B.E. and Ph.D. degrees in electrical engineering from Zhejiang University, Hangzhou, China, in 2015 and 2020, respectively.

From 2018 to 2019, he was a Visiting Scholar with the Advanced Research Institute, Virginia Tech, and also with the CURENT Center, University of Tennessee. He is currently an Assistant Professor with the State Key Laboratory of Internet of Things for Smart City, University of Macau, Macau, SAR, China. His research interests include optimization system, demand response, and Internet of Things technologies for smart energy.

and control of power systems, demand response, and Internet of Things technologies for smart energy.



Xia Chen (Member, IEEE) received the B.S. degree in power system and its automaton from the Wuhan University of Technology, China, in 2006, and the M.S. and Ph.D. degrees in electrical engineering from the Huazhong University of Science and Technology (HUST), China, in 2008 and 2012, respectively. She was a Postdoctoral Research Fellow with the University of Hong Kong from 2012 to 2015. In 2015, she joined HUST, where she is currently a Professor with the School of Electrical and Electronic Engineering. Her research interests include energy storage control and operation, renewable energy integration technologies, and new smart grid device.

and control of power systems, demand response, and Internet of Things technologies for smart energy.



Yonghua Song (Fellow, IEEE) received the B.E. degree in electrical engineering from the Chengdu University of Science and Technology, Chengdu, China, in 1984, and the Ph.D. degree in electrical engineering from China Electric Power Research Institute, Beijing, China, in 1989.

From 1989 to 1991, he was a Postdoctoral Fellow with Tsinghua University, Beijing, China. He then held various positions with Bristol University, Bristol, U.K.; Bath University, Bath, U.K.; and John Moores University, Liverpool, U.K., from 1991 to 1996. In 1997, he was a Professor of Power Systems with Brunel University, where he has been a Pro-Vice Chancellor for Graduate Studies since 2004. In 2007, he took up a Pro-Vice Chancellorship and Professorship of Electrical Engineering with the University of Liverpool, Liverpool. In 2009, he was with Tsinghua University as a Professor of Electrical Engineering and an Assistant President and the Deputy Director of the Laboratory of Low-Carbon Energy. From 2012 to 2017, he was the Executive Vice President of Zhejiang University, as well as the Founding Dean of the International Campus and a Professor of Electrical Engineering and Higher Education of the University. Since 2018, he has been a Rector of the University of Macau and the Director of the State Key Laboratory of Internet of Things for Smart City. His current research interests include smart grid, electricity economics, and operation and control of power systems.

Dr. Song was the recipient of D.Sc. by Brunel University in 2002, Honorary D.Eng. by the University of Bath in 2014, and Honorary D.Sc. by the University of Edinburgh in 2019. He was elected as the Vice-President of Chinese Society for Electrical Engineering (CSEE) and appointed as the Chairman of the International Affairs Committee of the CSEE in 2009. In 2004, he was elected as a Fellow of the Royal Academy of Engineering, U.K. In 2019, he was elected as a Foreign Member of the Academia Europaea.